Picosecond laser-pump, x-ray probe spectroscopy of GaAs

B. W. Adams[a)]
Advanced Photon Source, Argonne National Laboratory, Argonne, Illinois 60439

M. F. DeCamp, E. M. Dufresne, and D. A. Reis
University of Michigan, Department of Physics, 500 E. University Drive, Ann Arbor, Michigan 48109

(Received 21 March 2002; accepted 23 August 2002)

A laser-pump, x-ray probe spectroscopic experiment is described, and the results are shown. The Ga K_α x-ray fluorescence following x-ray absorption, at the Ga K absorption edge was measured, and its increase due to excitation with subpicosecond pulses of laser light at 4.6 eV photon energy was determined. The x-ray absorption, and thus the fluorescence, is increased for about 200 ps after the laser pulse because additional final states for the x-ray absorption are cleared in the valence band by the laser excitation. The technique could eventually lead to a femtosecond pump-probe spectroscopy with an absolute reference energy level and also to a femtosecond x-ray detector. This is of particular importance to future short-pulse x-ray sources, such as free-electron lasers. © *2002 American Institute of Physics.* [DOI: 10.1063/1.1516849]

I. INTRODUCTION

Within the last decade, the field of femtosecond laser spectroscopy has flourished tremendously because scientific interest met with advances in instrumentation: The time constants of electron dynamics in molecules and in condensed matter are of the order of picoseconds down to a few femtoseconds, and this domain is served by state-of-the-art laser systems, such as the mode-locked Ti:sapphire laser. That story may well be replayed when ultrashort pulses of x-rays become available at sufficient intensities. Laser/x-ray pump-probe spectroscopy can provide valuable information on electron dynamics that techniques based solely on near-visible light cannot yield. This applies to both structural information at atomic length scales and to element-specific spectroscopy. Because atomic transitions at x-ray frequencies refer to discrete energy levels in inner atomic shells, such a spectroscopy does not entail a convolution over intermediate states, as in visible-visible light pump-probe spectroscopy.

Laser/x-ray pump/probe experiments are only beginning to enter the mainstream of synchrotron radiation techniques.[1–4] With storage-ring-based sources, the time resolution is normally limited by the bunch length, which is tens of picoseconds at the three third-generation hard x-ray sources (European Synchrotron Radiation Facility (ESRF), Advanced Photon Square Synchrotron (APS), SPring8). An exception is the pulse-slicing beamline at the Advanced Light Source in Berkeley (ALS),[5] which reaches 300 fs at the expense of a low intensity. One may also use a streak camera to achieve down to subpicosecond time resolution, but at a low detection efficiency. Future sources, such as free-electron lasers[6,7] or energy-recovering linacs[8] will have significantly shorter bunches (80 fs at TESLA), but technological constraints are expected to place a lower limit of approximately one picosecond on the synchronization between lasers and x-rays. A way to overcome that limit is to measure the relative timing between laser and x-rays for each event with a femtosecond-resolving detector and bin the data into its respective time slot, see Ref. 9.

Here, we report on a picosecond-resolving laser-pump, x-ray probe experiment on GaAs, performed at the Advanced Photon Source Synchrotron. The results are a step towards both an ultrafast spectroscopy of carrier relaxation dynamics in condensed matter, and an ultrafast x-ray detector.

II. BACKGROUND

The following discussion is restricted to the case of GaAs. Much of it could however also be applied to many other materials, not even necessarily semiconductors (see Sec. V). Optical and terahertz radiation techniques have already yielded a great deal of information on the electron dynamics in GaAs and related substances, and a fairly good theoretical understanding of the relaxation processes has been developed. Theoretical studies have to take into account the scattering of carriers from phonons[10] (and for alloys, the disorder potential), multicarrier effects such as screening,[11] carrier–carrier scattering,[12] correlations,[13] and band-structure deformations.[14] A sampling of commonly used experimental techniques are two-photon luminescence,[15–18] two-photon absorption with two laser pulses,[19,20] or lasers and terahertz radiation.[21,22]

All these pump-probe techniques operate only within the band structure and thus do yield only a convolution over an intermediate state. To eliminate the convolution, and thus gain direct information on the electronic density of states and occupation density, one could reference the pump or the probe process to a discrete level, instead of a band. The technique described here uses time-resolved x-ray absorption spectroscopy to probe the density of available (i.e., nonoccupied) states in the band structure, following a laser excitation. When x-rays are incident on a sample of GaAs, the Ga K_α, and K_β fluorescence yield increases rapidly as the x-ray photon energy is tuned through the Ga K absorption edge at

a)Electronic mail: ADAMS@MAIL.DESY.DE

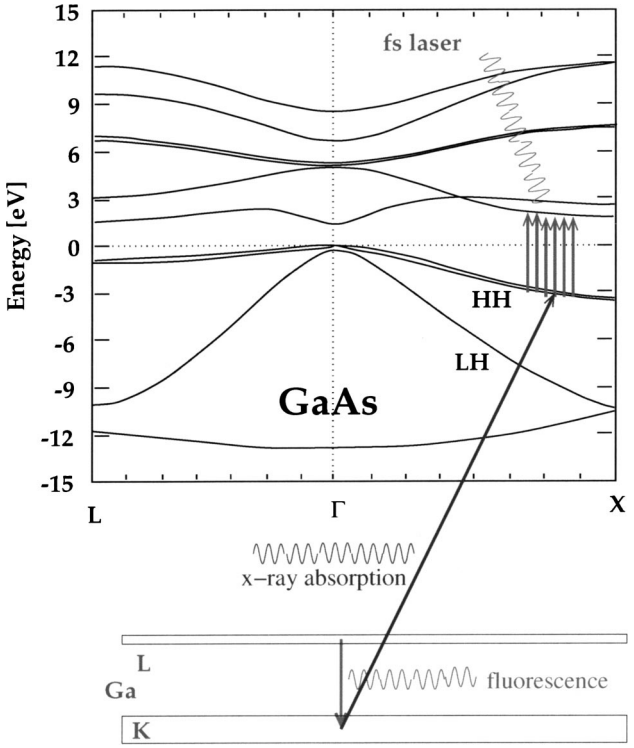

FIG. 1. Band structure of GaAs from Ref. 23 and core levels of Ga. The parallel arrows indicate the 4.6-eV laser-pump transition.

10.367 keV. Because of core-hole lifetime broadening, there is some fluorescence (or near-resonant Raman scattering) even if the incident energy is below the Ga K edge. When a short intense pulse of laser light transfers electrons from the valence to the conduction band, final states for the Ga K-shell x-ray absorption process are vacated in the valence band. Depending on the x-ray energy and where in the valence band these vacant states are, the cross section for the process of x-ray absorption, followed by fluorescence, may go up. This is indicated schematically in Fig. 1. Because of the strong interaction of the carriers with their environment, coherence of the excited carriers decays within femtoseconds. Any probe at longer time delays will therefore not see the excited state, but rather will follow the relaxation dynamics.

This process can be used to probe the laser-triggered dynamics of holes in the valence band with reference to an absolute energy level (i.e., Ga K), especially if a narrow-bandpass analyzer crystal is used for the fluorescent radiation to eliminate the core-hole lifetime effect.[24] Creation of the vacant states can occur within a few femtoseconds with a short-pulse laser, and the holes go out of range for the x-ray absorption process with appropriately monochromatized x-rays by *intra*-band relaxation within typically 100–200 fs. Therefore, the same principle can also be used for ultrafast x-ray detection. Details are described in Ref. 9. Corresponding to the APS pulse duration and jitter, the present experiment had a time resolution of approximately 100 ps, and femtosecond x-ray spectroscopy will require another type of source, such as a free-electron laser.

There are two distinct peaks in the light absorption spectrum of GaAs, one at about 3 eV and one at 4.6 eV, which are

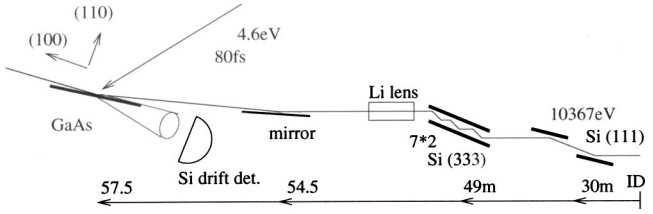

FIG. 2. Schematic of the beamline.

due to almost parallel portions of the band structure (see Fig. 1 and Refs. 23 and 25). For the femtosecond detector application, the pump laser should be tuned to one of these to create a large concentration of holes. The one at 4.6 eV is probably the better choice because the larger separation from the vacant states in the conduction band gives better contrast over the background fluorescence. On picosecond time scales (and thus for the experiment described below), the excitation energy should not matter very much because the carriers relax quickly to the direct band gap: The holes within 100 to 200 fs and the electrons in the conduction band within at most a few picoseconds (see Sec. V).

III. EXPERIMENT

The experiment was carried out at the 7-ID beamline of the APS (MHATT-CAT).[26] A Ti:sapphire laser system and electronics for the synchronization of the laser to the storage ring are installed in the D hutch of 7-ID, which is farthest from the source. The x-ray beamline shown in Fig. 2 is typical for a third-generation synchrotron radiation source, operating on an APS Type-A undulator.

A. X-ray optics

The Si(111) double crystal monochromator with cryo-cooled first crystal, at a point 30-m downstream from the source in the A hutch, was adjusted to the Ga K absorption edge at 10.367 keV. It provided approximately 5×10^{12} photons per second at 100 mA ring current. In order to obtain good energy resolution within the GaAs band structure, a Si (333) channel-cut crystal was inserted into the beam in the C hutch at a point 49 m from the source. Due to its higher reflection order, it narrowed the energy spread of the radiation transmitted to the sample (see Fig. 3) and the large number of 14 reflections in the channel (six of which are shown in Fig. 2) suppressed the wings of the reflectivity curve. By scanning the channel-cut angle and making use of the angular dispersion between the reflection orders (111) of the monochromator and (333) of the channel-cut, we could determine the angular divergence $\Delta\Theta^{(111)}$ in the monochromator output to be about 10% of the Si (111) rocking width, which puts the angle-correlated energy spread of the monochromator at about 0.15 eV. That 1.65-eV bandwidth coming from the monochromator is considerably narrowed down to approximately 0.17 eV by the (333) reflection, taking the divergence $\Delta\Theta^{(111)}$ into account (indicated by the wavelength range $\Delta\lambda_c$ in the DuMond diagram[27,28] in Fig. 3).

Right after the channel-cut crystal, a horizontally focusing compound refractive lithium lens[29] focused the x-rays onto the sample. A horizontally deflecting mirror suppressed

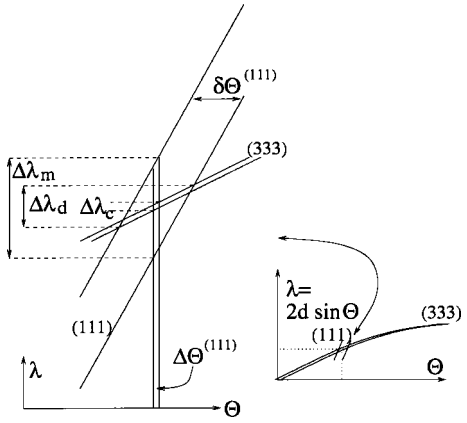

FIG. 3. Du Mond diagram to show the narrowing of the energy bandwidth by the (333) reflection of the channel-cut. $\delta\Theta^{(111)}$ and $\Delta\Theta^{(111)}$ are the rocking width of Si (111) and the divergence due to the thermal bump (see text). The wavelength spread for a plane incident wave with the (111) reflection only is $\Delta\lambda_m$. With the additional (333) reflection, one obtains $\Delta\lambda_c$ for a plane wave and $\Delta\lambda_d$ for a large incident divergence, respectively.

higher-order harmonics in the x-rays, which would otherwise lead to a considerable fluorescence background. Because the mirror and the lens were both placed after the monochromatizing elements, they did not cause any divergence-related spectral broadening.

B. Laser

The laser system consists of a mode-locked Ti:sapphire oscillator, an eight-pass Ti:sapphire laser amplifier, and some electronics to synchronize it to the storage ring rf (see Fig. 4). The laser oscillator is pumped by a continuous wave (cw) frequency-doubled Nd:VO_4 laser and runs at approximately 88 MHz repetition rate. It emits pulses of approximately 4 nJ in energy and approximately 50 fs in duration. The amplifier is pumped by a pulsed solid-state laser at 1 kHz repetition rate, and a Pockels cell selects appropriate pulses from the oscillator.

A set of nonlinear optical crystals was used to triple the optical photon energy in two steps: A beta barium borate (BBO) crystal converted part of the light from the Ti:sapphire laser at 820-nm center wavelength to the second harmonic, which was collinear with the fundamental. A potassium dihydrogen phosphate (KDP) crystal added the two components to create frequency-tripled light of 4.6 eV photon energy. The crystal parameters were not optimized for the purpose, but, nevertheless, pulses of about 1 μJ in the frequency-tripled light were produced. This light was focused to a footprint of about 0.5 by 5 mm on the sample. Rejection of the lower harmonics was assured by the use of dielectric mirrors in the beam path.

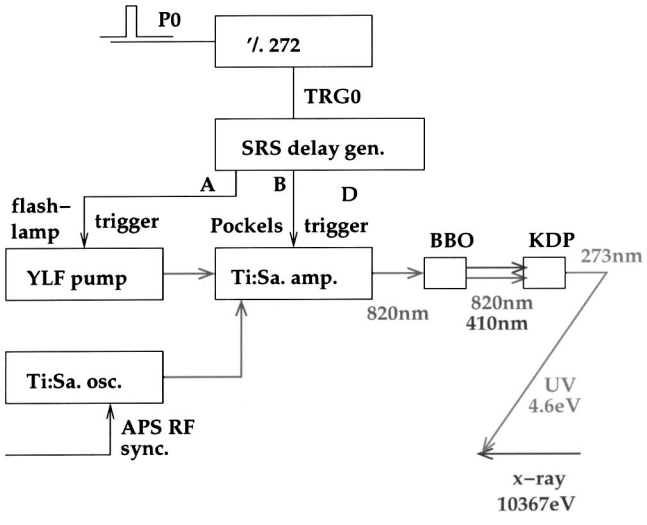

FIG. 4. Schematic of the laser system.

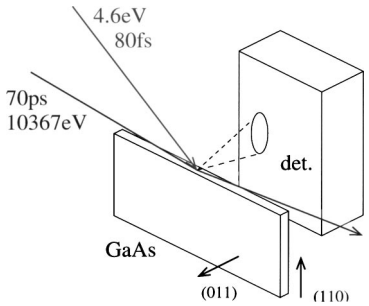

FIG. 5. Sample and detector.

C. Sample, detector

A (001) oriented GaAs wafer was cleaved to reveal a fresh (110) surface on its edge. It was mounted edge up in a diffractometer, so that the area it presented to the x-ray and laser beams was a narrow strip of 0.5 by 25 mm in the horizontal plane. Having such a restricted sample considerably facilitated the adjustment of spatial overlap between the x-ray and the laser beams. In order to match the penetration depth of the x-rays to that of the laser, the x-ray beam was made to hit the sample surface at an angle of about $1.05\alpha_c$, i.e., just above the critical angle α_c of total external reflection. Adjustment of the incidence angle was rather straightforward—the reflection off the cleaved surface was monitored on a fluorescent screen and α_c was determined both geometrically and by the drop in reflected intensity. The footprint of the x-ray beam on the sample was observable by the induced near-infrared luminescence that was visible to a charge coupled camera. The focus of the laser beam, incident at an angle of approximately 20° to the surface, gave an elongated footprint of approximately 0.5 by 2 mm. It was centered onto the x-ray footprint by use of the TV image and visual inspection on the spot. With the pulse energy in the UV laser light and the footprint area, we can roughly estimate the excitation energy density to be 10^{-4} J/cm^2, which is well below the damage threshold and should give rise to an initial carrier density of the order of 10^{19}/cm^3.

A silicon drift detector of type x-flash[30–32] was mounted so that its sensitive area of about 5 mm^2 was approximately 10 mm from the irradiated spot on the sample (see Fig. 5). It was positioned in the horizontal plane at approximately a right angle with respect to the incident x-rays. This geometry minimized the background of elastically scattered radiation, and the self-absorption suppressed radiation from deeper parts of the sample, which were not excited by the laser. Neither of these considerations was crucial—the elastic scat-

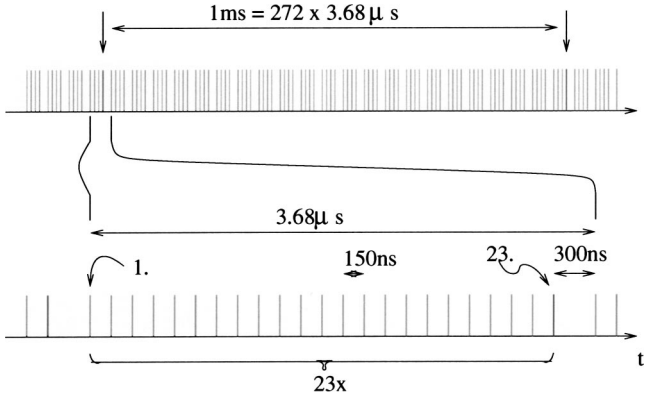

FIG. 6. The APS fill pattern. The upper trace represents 1 ms, or 272 round trips in the ring (abbreviated to 22 in the image), each giving off 23 bursts of x-rays (abbreviated to four in the image). The lower trace is a zoom into one such round trip.

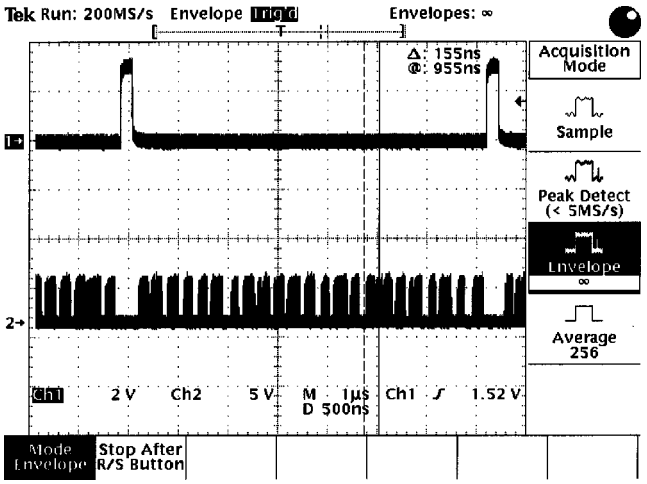

FIG. 7. Oscilloscope screen shot, upper trace: ring period clock PO; lower trace: output of the SCA in the detector signal chain. The oscilloscope was set to envelope mode to display SCA pulses belonging to all bunches on one screen. Single sweeps contained mostly no more than one SCA pulse.

tering was relatively weak in comparison to the Ga K fluorescence and the x-rays were depth-limited due to the grazing-incidence angle.

For each incident photon, the detector outputs a positive-going edge with a rise time of approximately 100 ns and an amplitude of 5 mV/keV. That raw output was taken out of the hutch by a doubly shielded BNC cable and fed into a Canberra 2025 filter amplifier, set to a shaping time constant of 500 ns. Despite the double shielding, the firing of the Pockels cell still was clearly visible in the input to the filter amplifier and was used for coarse timing adjustment (see below). Having the filter amplifier outside the hutch, rather than next to the detector, was the better choice for the following reason: The amplifier gain, as defined by the measured ratio of output amplitude to input amplitude, was about 160. Being an eight-pole filter,[33] the amplifier has an asymptotic high-frequency amplitude suppression of 24 dB per octave. The lowest frequency in the Pockels cell noise was about 20 MHz which is three to four octaves above the characteristic frequency of the filter amplifier, given by its shaping time constant. Therefore, the suppression of the Pockels cell noise is theoretically 3*24 dB and thus much stronger than the amplifier gain of about 22 dB. As the discussion in Sec. IV shows, a much more relevant frequency to suppress is of the order of 1.5 GHz.

D. Timing issues

Because the Ti:sapphire laser operates at a much lower repetition rate than the APS, only a small fraction of the x-rays contributed to the pump-probe signal, and the rest were used for normalization purposes. The fill pattern of the APS consisted of 23 bunches with 22 intervals of approximately 153 ns, and one of approximately 306 ns between them (see Fig. 6, lower part). The laser, operating at approximately 1 kHz repetition rate, was timed to the bunch that preceded the 300-ns dark interval (henceforth the 23rd bunch), once in 272 ring periods (see Fig. 6, upper part). With the Canberra 2025 amplifier in the signal chain, the Si drift detector can handle up to approximately 100 000 counts per second. Because the rate of x-ray pulses from the APS was 6.25×10^{6} s^{-1}, the incident intensity had to be limited to make the probability of one event in the detector about 1.6%. With the laser repetition rate at 1 kHz, this meant that the count rate from the bunches with laser could only be about 16 per second. A full discussion of count rate issues with a solid-state detector can be found in Ref. 34.

The timing synchronization involves two rather distinct mechanisms: The Ti:sapphire oscillator, running at a 88 MHz repetition rate, is synchronized directly to the accelerator rf, and the amplifier, running at 1 kHz, is triggered by a digital signal derived from the storage ring clock P0, which is a subharmonic of the accelerator rf at 272 kHz, corresponding to the ring period. Figure 4 shows a schematic of the timing circuitry, and in Fig. 7, an oscilloscope screen shot is shown with P0 in the upper trace and the output of the detector signal chain in the lower trace.

In a pump-probe experiment, it is imperative to achieve a good overlap between the pump and the probe beams in space (described above) and a stable and well-defined timing. Zero pump-probe delay was determined through the change in the Bragg reflectivity of germanium due to laser-induced acoustic phonons.[35]

After the timing was determined, the sample was installed and the fluorescence detector placed next to it, as shown in Fig. 5. Finally, the delay between the raw detector signal and the corresponding single-channel analyzer (SCA) output was determined, and the delay generator was programmed to provide a gate signal for a set of counters. This gate was logic-high at the times when an SCA output would occur from a bunch that the laser was timed to and was logic-low at all other times. Two digital counters with gate conditions of opposite polarity were then used to record the x-ray fluorescence with and without laser.

IV. RESULTS

We calibrated the monochromator with the Ga absorption edge by measuring the fluorescence with the drift detector positioned in the same way as later in the acquisition of the pump-probe data. Figure 8 shows one energy scan with

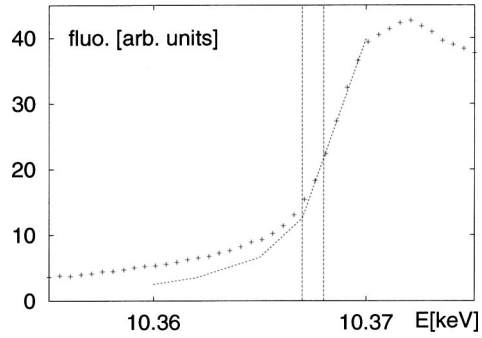

FIG. 8. Energy calibration. Crosses: energy scan with main monochromator only; dotted line: peak intensities of channel-cut scans at given monochromator energy setting. The intensity scale from 0 to 40 000 refers to the scan without channel-cut, the peak intensities through the channel-cut were less by a factor of ca. 0.1. The two vertical lines indicate the incident photon energies used in the experiment.

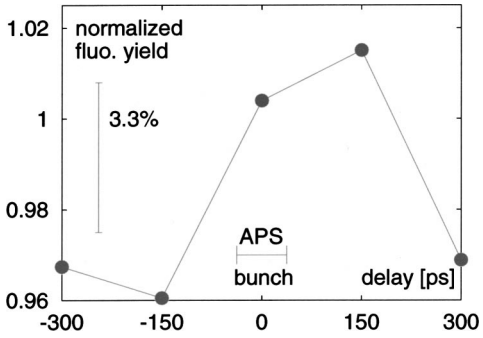

FIG. 10. Laser timing scan over ±300 ps at 10.367 keV incident photon energy (indicated by the right vertical line in Fig. 8). The error bar represents the 1σ Poisson counting statistics (see text), and the horizontal bar shows the FWHM bunch length of the APS.

the monochromator alone and one of peak intensities in channel-cut scans for the given monochromator energies. As can be seen in Fig. 8, the channel-cut suppresses the fluorescence yield at the lower end of the curve. However, the slope of the curve remains unchanged when the channel-cut is inserted because the Ga K and L core-hole lifetime broadening is larger than the energy bandpass of the Si (111) monochromator.

Due to the above-mentioned count rate restriction, the amount of data that could be taken in the approximately 1 1/2 days of raw data acquisition time was rather limited, and all the scans over ±300 ps are shown in Figs. 9 and 10. Both of them show averages of multiple intensity-normalized scans of the laser timing relative to the x-ray pulses. Each of these scans consists of five points, representing delays between laser and x-rays of −300, −150, 0, +150, and +300 ps. Negative values mean that the laser pulse comes after the x-rays. In Fig. 9, the average is made up of 17 individual scans at an incident nominal photon energy of 10.368 keV (see Fig. 8 for the energy calibration), and, in Fig. 10, the average consists of seven individual scans at an incident nominal photon energy of 10.367 keV. These two energies were chosen by the following reasoning: The inflection point of the energy calibration curve at 10.369 keV should correspond to the lower edge of the conduction band and the upper edge of the valence band where the holes accumulate within 100 to 200 fs after excitation is approximately 1.5 eV lower (see Sec. II) at 10.3675 keV on the calibration curve. The two energies in the experiment were chosen to bracket that point. The intensity normalization was done by dividing, for each point in each scan separately, the counts ''with laser'' by those ''without laser,'' and multiplying by 6250 (the ratio of x-ray pulses ''without laser'' to those ''with laser''). The modulation of the signal in Figs. 9 and 10 is about 4.5 and 3.5%, respectively which is more than the Poisson counting statistics of 1.95 and 3.3%. The latter values are obtained by taking the number of actual counts ''with laser'' represented by each of the points in Figs. 9 and 10 which are roughly 2650 and 910, respectively. The normalization counts are more than 6000 times more, and their effect on the counting statistics is negligible. The peaks of increased Ga K_α fluorescence in Figs. 9 and 10 have a width of about 250 ps. After taking into account the APS bunch length and jitter of together approximately 100 ps, the persistence of the fluorescence itself after laser excitation seems to be about 200 ps. The physics of these results is discussed in Sec. V.

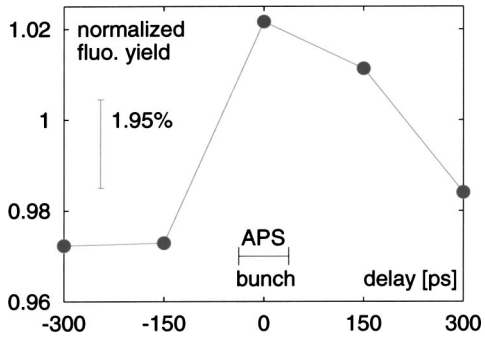

FIG. 9. Laser timing scan over ±300 ps at 10.368 keV incident photon energy (indicated by the left vertical line in Fig. 8). The error bar represents the 1σ Poisson counting statistics (see text), and the horizontal bar shows the full width at half maximum (FWHM) bunch length of the APS.

The baseline of the normalized fluorescence yield (i.e., the data points at negative times) in Figs. 9 and 10 is at approximately 0.97, instead of 1.0. This could be due to the 23rd bunch in the fill having a below-average charge. Five percent variations are normal.[36] Because the APS was not operating in the top-up mode at the time of the experiment, any such charge variations would persist until the next fill. Another possible explanation for the baseline deficit has to do with the details of the signal processing chain. It is conceivable that the SCA window was inadvertently set too tight and that the Pockels cell noise shifted the baseline of the signal from the detector just at the times when the laser fired. It is however hard to believe that the Pockels cell noise could have a 3% effect after being suppressed by approximately 70 dB (see Sec. III C). However, this brings up another question, namely, if the apparent increase in fluorescence yield in Figs. 9 and 10 could be an artifact due to the Pockels cell noise. That explanation seems however highly unlikely because the timing electronics was set up to scan the laser timing with the Ti:sapphire oscillator only and to keep the Pockels cell firing constant relative to the x-rays and the bunch clock. Furthermore, the duration of the increased fluorescence is of the order of 200 to 300 ps, corresponding to a

frequency of at least 1.5 GHz at which the suppression in the spectroscopy amplifier is even much stronger than the aforementioned 70 dB.

Brief mention should also be given here to a pump-probe experiment that was conducted at beamline ID9 of the European Synchrotron Radiation Facility (ESRF) and yielded inconclusive results. There were a few differences in the ways that the APS and ESRF experiments were done, which shall be discussed briefly: ID9 had a focusing mirror before the monochromator, which gave rise to a vertical divergence, and thus an energy spread in the monochromator, which we measured to be several electronvolts (the beamline configuration has recently been changed, and the focusing mirror comes now after the monochromator[37]). However, a Si (333) channel-cut crystal was used at ID9, too, and the energy bandpass should be limited by $\Delta\lambda_d \approx 0.8$ eV (see Fig. 3), regardless of the divergence. The sample surface orientation was different in the two experiments, namely, (111) at the ESRF and (220) at the APS. It is known that the carrier recombination proceeds much faster near a surface than it does in the bulk and the orientation plays a role. At ID9,[38] the laser photon energy was only doubled, not tripled. The laser absorption at 4.6 eV should be a bit stronger than at 3 eV (see Ref. 25, Fig. 1), but not dramatically so. On the other hand, the ESRF experiment was done close to the laser damage threshold of GaAs, whereas, at the APS, we stayed below it by at least a factor of 10. For both laser photon energies, the charge carriers should relax to the same state, with the holes reaching the top of the valence band within approximately 200 fs and electrons scattering from the *L* or *X* minimum to the absolute minimum at Γ within a few picoseconds (see Sec. V). This means that the excitation energy should play no role on timescales beyond the picosecond relaxation time. If that is truly so, it will have to be clarified in further experiments (see Sec. V below).

V. DISCUSSION AND OUTLOOK

The dynamics of carrier photoexcitation and subsequent relaxation in GaAs and related substances is rather complicated because of the multitude of branches within the band structure and because different relaxation processes play a role, their relative influence depending on details like excitation density, initial energy distribution, etc. Roughly speaking, the sequence of events is as follows. Absorption of laser photons takes electrons from the valence to the conduction band in a transition that is predominantly direct (i.e., almost vertical within the band structure), but can also involve the excitation of large-momentum excitons[39] if excess energy of the right magnitude (several hundred milli-electron volts) is available from the photons. Right after a direct transition, quantum coherence of the carriers exists, as demonstrated, for example, by quantum beats in absorption.[40] Quantum coherence is lost within tens of femtoseconds and the initial nonequilibrium carrier distribution relaxes within typically tens to hundreds of femtoseconds towards a hot thermal distribution.[41] The dominant dissipation mechanisms are carrier–carrier scattering for high-, and carrier-photon scattering for low-excitation densities, respectively. The elementary time constant of the former is given by the plasma frequency $\omega_p^2 = 4\pi c^2 r_e \rho$ (approximately 50 fs at a carrier density of $\rho = 5 \times 10^{18}$ cm^{-3}), but with some modification due to screening effects. For the latter, the elementary time constant is typically 100 to 200 fs (the LO phonon in GaAs has a period of approximately 115 fs). Experiments[42,43,41] indicate even shorter time constants which might be explained by quantum kinetic processes.[43] Finally, full recombination across the direct band gap takes typically hundreds of picoseconds (see Ref. 22, Fig. 7). Because the estimated excitation density of the present experiment was about 10^{19} cm^{-3}, the thermalization should be determined by carrier–carrier interactions. It should however be pointed out that the data cited above applies to carriers that are not more than a few hundred milli-electron volts away from the band edges. In the present experiment, the holes are initially created several electron volts below the band edge, but that should not slow the thermalization significantly down.

The results in Figs. 9 and 10 therefore seem to be an increase in fluorescence, due to an increase in the absorption cross section just below the Ga absorption edge, which is caused by the holes that accumulate at the top of the valence band. This signal persists as long as the holes are not yet eliminated by recombination. The duration of the increased fluorescence yield is approximately 200 to 300 ps, which is in agreement with typical recombination times, as seen, for example, in terahertz absorption measurements.[21,22]

Further progress will depend on improvements of the energy resolution to well below the width of the band structure. This is obviously necessary for a spectroscopic method to resolve processes within the band structure, and the femtosecond detector[9] also needs to resolve states deep within the valence band to make use of the fast intraband relaxation for closure of the window of sensitivity. In the current setup, the energy resolution is limited by the core-hole lifetime broadening (see Sec. IV). A possible way to eliminate the lifetime effect of the K hole, leaving only a residual broadening due to the upper level in the fluorescence, would be to use an analyzer crystal for the fluorescent x-rays.[24,44] It would then be advantageous to look at x-ray fluorescence due to a transition from a shallow core state (such as K_β from the *M* level in Ga), instead of K_α, to minimize the residual core-hole lifetime broadening.

Such an analyzer will need to resolve better than one electron volt and collect fluorescence from a large solid angle. That is certainly not trivial, however, the inelastic x-ray scattering instruments at the major synchrotron radiation facilities do routinely reach milli-electron volts resolution with similar analyzers. Both the spectroscopic application and the femtosecond detector are worth some development effort: Two-photon experiments using only low-energy (visible, IR, terahertz) photons give only a convolution over the intermediate state. In contrast, the technique demonstrated here provides an absolute energy reference level by making use of a core state. It can therefore provide much more detailed information on electron dynamics in solid matter. A femtosecond-resolving detector will be absolutely necessary to open the ultrashort science possibilities[45] of x-ray free-electron lasers and energy-

recovery linacs. As of now, there are only a few ideas, such as making use of laser-assisted x-ray photoelectron emission[46] or the concept presented here and in Ref. 9. Given the above data on thermalization of photoexcited carriers at high-excitation densities, such a detector should be capable of reaching better than 100 fs time resolution.

ACKNOWLEDGMENTS

Operation of the MHATT-CAT sector 7 beamline at the Advanced Photon Source was supported by DOE Grant Nos. DE-FG02-99ER45743 and DE-FG02-00ER15031. Use of the APS and one of us (B.W.A.) were supported by the U.S. Department of Energy under Contract No. W-31-109-ENG-38. We want to thank D. Arms for his support of the experiment at the APS, and D. Lowney and T. Plech for their assistance at the ESRF.

[1] M. DeCamp *et al.*, Nature (London) **413**, 825 (2001).
[2] S. Techert, F. Schotte, and M. Wulff, Phys. Rev. Lett. **86**, 2030 (2001).
[3] R. Neutze *et al.*, Phys. Rev. Lett. **87**, 195 508 (2001).
[4] C. Bressler *et al.*, JCP **116**, 2955 (2002).
[5] R. Schoenlein *et al.*, Synchrotron Radiat. News **14**, 20 (2001).
[6] J. Arthur, G. Materlik, R. Tatchyn, and H. Winick, Rev. Sci. Instrum. **66**, 1987 (1995).
[7] J. Schneider, Nucl. Instrum. Methods Phys. Res. A **398**, 41 (1997).
[8] H. Padmore, R. Schoenlein, and A. Zholents, Synchrotron Radiat. News **14**, 26 (2001).
[9] B. Adams, Nucl. Instrum. Methods Phys. Res. A **459**, 339 (2001).
[10] A. Leitenstorfer *et al.*, Phys. Rev. Lett. **76**, 1545 (1996).
[11] J. Collet, Phys. Rev. B **47**, 10 279 (1993).
[12] N. Nintunze and M. Osman, Phys. Rev. B **50**, 10 706 (1994).
[13] D. Snoke, W. Rühle, and Y.-C. L. E. Bauser, Phys. Rev. B **45**, 10 979 (1992).
[14] M. Cavicchia and R. Alfano, Phys. Rev. B **48**, 5696 (1993).
[15] R. Kumar and A. Vengurlekar, Phys. Rev. B **54**, 10 292 (1996).
[16] R. Kumar *et al.*, Phys. Rev. B **54**, 17 591 (1996).
[17] K. Burr and C. Tang, Appl. Phys. Lett. **74**, 1734 (1999).
[18] T. Elsaesser, J. Shah, L. Rota, and P. Lugli, Phys. Rev. Lett. **66**, 1757 (1991).
[19] E. Mayer, A. Lohner, M. Woerner, and T. Elsaesser, Phys. Rev. B **46**, 1878 (1992).
[20] S. Hunsche *et al.*, Phys. Rev. B **48**, 17 818 (1993).
[21] A. Vengurlekar and S. Jha, Phys. Rev. B **41**, 1286 (1990).
[22] M. Beard, G. Turner, and C. Schmuttenmaer, Phys. Rev. B **62**, 15 764 (2000).
[23] T. Boykin, Phys. Rev. B **54**, 8107 (1996).
[24] K. Hämäläinen, D. Siddons, J. Hastings, and L. Berman, Phys. Rev. Lett. **67**, 2850 (1991).
[25] E. Glezer, Y. Siegal, L. Huang, and E. Mazur, Phys. Rev. B **51**, 6959 (1995).
[26] E. Dufresne *et al.*, Rev. Sci. Instrum. **73**, 1511 (2002).
[27] J. DuMond, Phys. Rev. **52**, 872 (1937).
[28] T. Matsushita and H. Hashizume, in *Handbook of Synchrotron Radiation*, edited by E. Koch (North-Holland, Amsterdam, 1983), Vol. 1, Chap. 4.
[29] E. Dufresne *et al.*, Appl. Phys. Lett. **79**, 4085 (2001).
[30] G. Röntec AG, Berlin, Röntec X-Flash detector, details on http://www.roentec.de, 1997.
[31] C. Fiorini *et al.*, Rev. Sci. Instrum. **68**, 2461 (1997).
[32] C. Fiorini *et al.*, J. X-Ray Sci. Technol. **7**, 117 (1997).
[33] Canberra, Canberra, Inc., specifications of model 2025 AFT research amplifier, http://www.canberra.com/PCatalog.nsf/all/NIM_PDF/$file/3m2025.pdf, 2001.
[34] G. Jennings, W. Jäger, and L. Chen, Rev. Sci. Instrum. **73**, 362 (2002).
[35] D. Reis *et al.*, Phys. Rev. Lett. **86**, 3072 (2001).
[36] G. Decker, APS accelerator division (private communication, 2002).
[37] S. Techert *et al.*, in *Winter School Les Houches* (ESRF, http://www.esrf.fr/conferences/FEL_SR/Introduction.htm, 2001).
[38] M. Wulff *et al.*, Nucl. Instrum. Methods Phys. Res. A **398**, 69 (1997).
[39] G. Göger *et al.*, Phys. Rev. Lett. **84**, 5812 (2000).
[40] M. Joschko *et al.*, Phys. Rev. B **58**, 10 470 (1998).
[41] A. Alexandrou, V. Berger, and D. Hulin, Phys. Rev. B **52**, 4654 (1995).
[42] F. Ganikhov, K. Burr, and C. Tang, Appl. Phys. Lett. **73**, 64 (1998).
[43] S. Bar-Ad *et al.*, Phys. Rev. Lett. **77**, 3177 (1996).
[44] P. Carra, M. Fabrizio, and B. Thole, Phys. Rev. Lett. **74**, 3700 (1995).
[45] In TESLA technical design report, Part V, http://tesla.desy.de/new_pages/TDR_CD/PartV/fel.html,DESY, edited by G. Materlik and T. Tschentscher (DESY, Notkestr. 85, D-22607 Hamburg, Germany, 2001).
[46] T. Glover, R. Schoenlein, A. Chin, and C. Shank, Phys. Rev. Lett. **76**, 2468 (1996).